TRANSACTIONS OF THE ASME

JOURNAL OF FLUIDS ENGINEERING

PUBLISHED QUARTERLY BY THE AMERICAN SOCIETY OF MECHANICAL ENGINEERS • MARCH 2002

Approach for Input Uncertainty Propagation and Robust Design in CFD Using Sensitivity Derivatives[1]

Michele M. Putko
Ph.D. Candidate

Arthur C. Taylor III
Associate Professor

Department of Mechanical Engineering,
Old Dominion University,
Norfolk, VA 23529

Perry A. Newman
Senior Research Scientist

Lawrence L. Green
Research Scientist

NASA Langley Research Center,
Hampton, VA 23681

An implementation of the approximate statistical moment method for uncertainty propagation and robust optimization for quasi 1-D Euler CFD code is presented. Given uncertainties in statistically independent, random, normally distributed input variables, first- and second-order statistical moment procedures are performed to approximate the uncertainty in the CFD output. Efficient calculation of both first- and second-order sensitivity derivatives is required. In order to assess the validity of the approximations, these moments are compared with statistical moments generated through Monte Carlo simulations. The uncertainties in the CFD input variables are also incorporated into a robust optimization procedure. For this optimization, statistical moments involving first-order sensitivity derivatives appear in the objective function and system constraints. Second-order sensitivity derivatives are used in a gradient-based search to successfully execute a robust optimization. The approximate methods used throughout the analyses are found to be valid when considering robustness about input parameter mean values.
[DOI: 10.1115/1.1446068]

1 Introduction

Gradient-based optimization of complex aerodynamic configurations and their components, utilizing high-fidelity Computational Fluid Dynamics (CFD) tools, continues as a very active area of research (see, for example, [1–3]). In most of the CFD-based aerodynamic optimization and design studies to date, the input data and parameters have been assumed precisely known; we refer to this as deterministic or conventional optimization. When statistical uncertainties exist in the input data or parameters, however, these uncertainties affect the design and therefore must be accounted for in the optimization. Such optimizations under uncertainty have been studied and used in structural design disciplines (see, for example [4–8]); we refer to these as nondeterministic or robust design optimization procedures.

Derivatives of code output with respect to code input and parameters are called sensitivity derivatives and they contain information which can be used to direct an optimization search. In a fluid flow optimization problem, the objective and constraint gradients are functions of the CFD sensitivity derivatives. Such derivatives can also be used to accurately approximate the CFD output in a small region, such as that near the mean value of a random variable. In [9], it is shown that a statistical First Order Second Moment (FOSM) method and automatic differentiation can be used to efficiently propagate input uncertainties through finite element analyses to approximate output uncertainty. This uncertainty propagation method is demonstrated herein for CFD code.

An integrated strategy for mitigating the effect of uncertainty in simulation-based design is presented in [10]; this strategy consists of uncertainty quantification, uncertainty propagation, and robust design tasks or modules. Two approaches are discussed there for propagating uncertainty through sequential analysis codes: an extreme condition approach and a statistical approach. Both approaches can be efficiently implemented using sensitivity derivatives. For CFD code, the former approach is demonstrated in [11], whereas the latter approach is demonstrated herein using second moment approximations. These uncertainty propagation methods have been developed and are being investigated as an alternative to propagation by direct Monte Carlo simulation for potentially expensive CFD analyses.

The present paper shows how the approximate statistical second moment methods, FOSM and the Second Order Second Moment (SOSM) counterpart, can be used in conjunction with sensitivity derivatives to propagate input data uncertainties through CFD code to estimate output uncertainties. The FOSM approximation is then used to perform sample robust optimizations. For demonstration purposes, the method is illustrated on a simple design example which contains the important elements of more complex design problems. We assume that the input uncertainty quantification is given by independent normally-distributed random variables, and we demonstrate the strategy of [10] as applied to a CFD code module. This strategy is also applicable to correlated and/or non-normally distributed variables; however, the analysis and resulting equations become much more complex.

The gradient-based robust optimization demonstrated herein requires second-order sensitivity derivatives from the CFD code. In [12], we present, discuss, and demonstrate the efficient calculation of second-order derivatives from CFD code using a method proposed, but not demonstrated, in [13]. This method, used herein, incorporates first-order derivatives obtained by both forward-mode and reverse-mode differentiation in a noniterative scheme to obtain second-order sensitivity derivatives.

To date, the only other demonstration or application of gradient-based, robust optimization involving advanced or high-fidelity (nonlinear) CFD code that we have found was just recently presented in [14–15]. The analytical statistical approximation of their objective function for robust optimization also required second-order sensitivity derivatives. However, these studies employed a direct numerical random sampling technique to compute expected values at each optimization step in order to

[1]This paper is declared a work of the U.S. Government and is not subject to copyright protection in the United States.

Contributed by the Fluids Engineering Division for publication in the JOURNAL OF FLUIDS ENGINEERING. Manuscript received by the Fluids Engineering Division July 20, 2001; revised manuscript received November 12, 2001. Associate Editor: G. Karniadakis.

avoid the second derivatives. An example of linear aerodynamics involved in multidisciplinary performance optimization subject to uncertainty is found in [16].

Two other aspects need to be pointed out in regard to the robust optimization demonstrations for CFD code modules presented herein and also in [14,15]. First, the sources of uncertainty considered were only those due to code input parameters involving geometry and/or flow conditions; i.e., due to sources external to the CFD code simulation. Other computational simulation uncertainties, such as those due to physical, mathematical, and numerical modeling approximations [17,18]—essentially internal model error and uncertainty sources, were not considered. That is, the discrete CFD code analysis results were taken to be deterministically "certain" herein. Ultimately, all of these modeling sources of error and uncertainty must be assessed and considered. Sensitivity derivatives can also aid in this assessment [19] since the adequacy of an internal model's (i.e., algorithm, turbulence, etc.) prediction capability generally depends, to some extent, on the modeling parameter values specified as input.

Second, as discussed in [15], uncertainty classification with respect to an event's impact (from performance loss to catastrophic) and frequency (from everyday fluctuation to extremely rare) sets the problem formulation and solution procedure. Structural reliability techniques typically deal with risk assessment of infrequent but catastrophic failure modes, identifying the most probable point of failure and its safety index. Here, we are addressing the assessment of everyday operational fluctuations on performance loss, not catastrophe. Consequently, we are most concerned with aero performance behavior due to probable fluctuations, i.e., near the mean of probability density functions (pdf). Structural reliability assessment is most concerned with improbable catastrophic events, i.e., probability in the tails of the pdf. Simultaneous consideration of both types of uncertainty is discussed in [16].

2 Integrated Statistical Approach

In [10] an integrated methodology for dealing with uncertainty in a simulation-based design is proposed and demonstrated for a linkage mechanism design. The integrated strategy of [10] for mitigating the effect of uncertainty includes (a) uncertainty quantification, (b) uncertainty propagation, and (c) robust design. The present study utilizes the strategy proposed in [10], but differs in regard to uncertainty propagation and application. Here, we are considering the influence of uncertainty in CFD code input: that is, the effect of uncertainty in input geometry on aerodynamic shape-design optimization and the effect of uncertainty in flow conditions on design for flow control.

2.1 Uncertainty Quantification. In this study, we consider the influence of uncertainty in CFD input parameterization variables. We have assumed that these input variables are statistically independent, random, and normally distributed about a mean value. This assumption not only simplifies the resulting algebra and equations, but also serves to quantify input uncertainties. Furthermore, it is not an unreasonable assumption for input geometric variables subject to random manufacturing errors nor for input flow conditions subject to random fluctuations.

2.2 Uncertainty Propagation. Uncertainty propagation is accomplished by approximate statistical second moment methods [9] and [20] where the required sensitivity derivatives are obtained by hand or by automatic differentiation. The first step in second moment analyses is to approximate the CFD system output solutions of interest in Taylor series form, truncated to the desired order. These approximations are formed to estimate the output value for small deviations of the input.

Given input random variables $\mathbf{b}=\{b_1,\ldots,b_n\}$ with mean values, $\bar{\mathbf{b}}=\{\bar{b}_1,\ldots,\bar{b}_n\}$, and standard deviations, $\sigma_{\mathbf{b}}=\{\sigma_{b_1},\ldots,\sigma_{b_n}\}$, first- and second-order Taylor series approximations of the CFD output function, $\mathbf{F}$, are given by

$$\mathbf{F}(\mathbf{b})=\mathbf{F}(\bar{\mathbf{b}})+\sum_{i=1}^{n}\frac{\partial\mathbf{F}}{\partial b_i}(b_i-\bar{b}_i) \tag{1}$$

and

$$\mathbf{F}(\mathbf{b})=\mathbf{F}(\bar{\mathbf{b}})+\sum_{i=1}^{n}\frac{\partial\mathbf{F}}{\partial b_i}(b_i-\bar{b}_i)+\frac{1}{2!}\sum_{j=1}^{n}\sum_{i=1}^{n}\frac{\partial^2\mathbf{F}}{\partial b_i\partial b_j}(b_i-\bar{b}_i)(b_j-\bar{b}_j), \tag{2}$$

respectively. Both first and second derivatives are evaluated at the mean values, $\bar{\mathbf{b}}$.

One then obtains expected values for the mean (first moment) and variance (second moment) of the output function, $\mathbf{F}$, which depend on the sensitivity derivatives and input variances, $\sigma^2_{\mathbf{b}}$. The mean of the output function, $\bar{\mathbf{F}}$, and standard deviation $\sigma_{\mathbf{F}}$, are approximated as

First Order:

$$\bar{\mathbf{F}}=\mathbf{F}(\bar{\mathbf{b}})$$

$$\sigma^2_{\mathbf{F}}=\sum_{i=1}^{n}\left(\frac{\partial\mathbf{F}}{\partial b_i}\sigma_{b_i}\right)^2 \tag{3}$$

Second Order:

$$\bar{\mathbf{F}}=\mathbf{F}(\bar{\mathbf{b}})+\frac{1}{2!}\sum_{i=1}^{n}\frac{\partial^2\mathbf{F}}{\partial b_i^2}\sigma^2_{b_i}$$

$$\sigma^2_{\mathbf{F}}=\sum_{i=1}^{n}\left(\frac{\partial\mathbf{F}}{\partial b_i}\sigma_{b_i}\right)^2+\frac{1}{2!}\sum_{j=1}^{n}\sum_{i=1}^{n}\left(\frac{\partial^2\mathbf{F}}{\partial b_i\partial b_j}\sigma_{b_i}\sigma_{b_j}\right)^2, \tag{4}$$

where both first and second derivatives are evaluated at the mean values, $\bar{\mathbf{b}}$. Note in Eq. (4) that the second-order mean output, $\bar{\mathbf{F}}$, is not at the mean values of input $\bar{\mathbf{b}}$, i.e., $\bar{\mathbf{F}}\neq\mathbf{F}(\bar{\mathbf{b}})$.

Equations (3) and (4) are the FOSM and SOSM approximations, respectively, for the uncertainty propagation. The methods are straightforward with the difficulty largely lying in computation of the sensitivity derivatives. The very efficient and effective method used here to obtain such derivatives is presented in [12].

2.3 Robust Design. Conventional optimization for an objective function, Obj, that is a function of the CFD output, $\mathbf{F}$, state variables, $\mathbf{Q}$, and input variables, $\mathbf{b}$, is expressed in Eq. (5). Herein, the CFD state equation residuals, $\mathbf{R}$, are represented as an equality constraint, and other system constraints, $\mathbf{g}$, are represented as inequality constraints. The input variables, $\mathbf{b}$, are precisely known, and all functions of $\mathbf{b}$ are therefore deterministic.

min Obj,

$$\mathrm{Obj}=\mathrm{Obj}(\mathbf{F},\mathbf{Q},\mathbf{b})$$

subject to

$$\mathbf{R}(\mathbf{Q},\mathbf{b})=0$$

$$\mathbf{g}(\mathbf{F},\mathbf{Q},\mathbf{b})\leq 0 \tag{5}$$

For robust design, the conventional optimization, Eq. (5), must be treated in a probabilistic manner. Given uncertainty in the input variables, $\mathbf{b}$, all functions in Eq. (5) are no longer deterministic. The design variables are now the mean values, $\bar{\mathbf{b}}=\{\bar{b}_1,\ldots,\bar{b}_n\}$, where all elements of $\bar{\mathbf{b}}$ are assumed statistically independent and normally distributed with standard deviations $\sigma_{\mathbf{b}}$. The objective function is cast in terms of expected values and becomes a function of $\bar{\mathbf{F}}$ and $\sigma_{\mathbf{F}}$. The state equation residual equality constraint, $\mathbf{R}$, is deemed to be satisfied at the expected values of $\mathbf{Q}$ and $\mathbf{b}$, that is the mean values $\bar{\mathbf{Q}}$ and $\bar{\mathbf{b}}$ for the FO approximation. The other constraints are cast into a probabilistic statement: the probability that the constraints are satisfied

is greater than or equal to a desired or specified probability, P_k. This probability statement is transformed [10] into a constraint involving mean values and standard deviations under the assumption that variables involved are normally distributed. The robust optimization can be expressed as
min Obj,

$$\text{Obj}=\text{Obj}(\bar{\mathbf{F}},\sigma_{\mathbf{F}},\bar{\mathbf{Q}},\bar{\mathbf{b}})$$

subject to

$$\mathbf{R}(\bar{\mathbf{Q}},\bar{\mathbf{b}})=0$$

$$\mathbf{g}(\bar{\mathbf{F}},\bar{\mathbf{Q}},\bar{\mathbf{b}})+k\sigma_{\mathbf{g}}\leq 0, \tag{6}$$

where k is the number of standard deviations, $\sigma_{\mathbf{g}}$, that the constraint $\mathbf{g}$ must be displaced in order to achieve the desired or specified probability, P_k. For the FOSM approximation, standard deviations $\sigma_{\mathbf{F}}$ and $\sigma_{\mathbf{g}}$ are of the form given in Eq. (3) involving first-order sensitivity derivatives. Therefore, a gradient-based optimization will then require second-order sensitivity derivatives to compute the objective and constraint gradients. Note that for the SOSM approximation, third-order sensitivity derivatives would be required for these gradients.

The calculation of second-order sensitivity derivatives for CFD code, such as those required for SOSM and robust optimization with FOSM, was demonstrated in [13]; the efficient calculation method used herein is demonstrated and discussed in [12]. Both hand differentiation and automatic differentiation via the ADIFOR tool [21–23] were used in [12] and [13]. Both conventional and robust optimizations were performed using the Sequential Quadratic Programming method option in the Design Optimization Tools, DOT [24].

3 Application to Quasi 1-D Euler CFD

A very simple example has been chosen to demonstrate the propagation of input uncertainty through CFD code and its effect on optimization. The quasi one-dimensional Euler equations and approximate boundary conditions are solved in a discretized CFD form (see Appendix). Of course, modern CFD methods are not required to solve the quasi 1-D Euler equations; exact analytical solutions are available in any basic textbook on gas dynamics. However, these quasi 1-D equations are commonly and effectively used as the initial test platform in the development of CFD algorithms and methods.

Two separate applications are presented: the first involving propagation of geometric uncertainties, the second involving propagation of flow parameter uncertainties. Both uncertainty analyses are performed with quasi one-dimensional CFD Euler equations and boundary conditions describing subsonic flow through a variable area nozzle. The nozzle inlet is located at $x=0$ with area $A(x=0)=1$; the nozzle outlet is at $x=1$. The area distribution is given by

$$A(x)=1-ax+bx^2.$$

The volume, V, occupied by the nozzle, is the integration of $A(x)$ over the length $x=0$ to $x=1$

$$V=1-\frac{a}{2}+\frac{b}{3},$$

where a and b are the input geometric parameters. Three flow parameters are specified as input boundary conditions: the stagnation enthalpy, inlet entropy, and outlet static (back) pressure. The discretized quasi 1-D Euler equation set is symbolically written as the state equation in Eq. (5); its residual, $\mathbf{R}$ is driven to (machine) zero for a solution (see Appendix).

For supersonic flow through a variable area nozzle, shock waves generally appear and the flow solution (objective, constraint, etc.) becomes noisy or non-smooth (see [25] and the references cited therein). Care must be exercised with respect to obtaining and using the sensitivity derivatives needed for gradient-based optimization [25,26]. Therefore, we chose to bypass issues related to this supersonic flow non-smoothness in these initial demonstrations of the present approach for uncertainty propagation and robust design for CFD code modules.

3.1 Geometric Uncertainty Propagation. For the discussion of geometric uncertainty propagation, geometric shape parameters a and b will represent the statistically independent random input variables, $\mathbf{b}$. The Mach number distribution through the nozzle, $\mathbf{M}$, is viewed here as a component of the state variable, $\mathbf{Q}$; its value at the inlet, $\mathbf{M}$, is the CFD output, $\mathbf{F}$. Applying the approach previously outlined (recall Eqs. (3) and (4)) yields the following first-and second-order approximations of the output function, $\mathbf{M}$.
Input random variables: $\mathbf{b}=\{a,b\}$
CFD output function: $\mathbf{F}=\{\mathbf{M}\}$
First-order Taylor series:

$$\mathrm{M}(a,b)=\mathrm{M}(\bar{a},\bar{b})+\frac{\partial \mathrm{M}}{\partial a}(a-\bar{a})+\frac{\partial \mathrm{M}}{\partial b}(b-\bar{b}) \tag{7}$$

Second-order Taylor series:

$$\mathrm{M}(a,b)=M(\bar{a},\bar{b})+\frac{\partial \mathrm{M}}{\partial a}(a-\bar{a})+\frac{\partial \mathrm{M}}{\partial b}(b-\bar{b})+\frac{\partial^2 \mathrm{M}}{\partial a\,\partial b}(a-\bar{a})$$
$$\times(b-\bar{b})+0.5\left(\frac{\partial^2 \mathrm{M}}{\partial a^2}(a-\bar{a})^2\right)+0.5\left(\frac{\partial^2 \mathrm{M}}{\partial b^2}(b-\bar{b})^2\right) \tag{8}$$

The mean, $\bar{\mathrm{M}}$, and standard deviation σ_M of the output function are expressed as
FOSM:

$$\bar{\mathrm{M}}=\mathrm{M}(\bar{a},\bar{b})$$
$$\sigma_M^2=\left(\frac{\partial \mathrm{M}}{\partial a}\sigma_a\right)^2+\left(\frac{\partial \mathrm{M}}{\partial b}\sigma_b\right)^2 \tag{9}$$

SOSM:

$$\bar{\mathrm{M}}=\mathrm{M}(\bar{a},\bar{b})+0.5\left(\frac{\partial^2 \mathrm{M}}{\partial a^2}\right)\sigma_a^2+0.5\left(\frac{\partial^2 \mathrm{M}}{\partial b^2}\right)\sigma_b^2$$
$$\sigma_M^2=\left(\frac{\partial \mathrm{M}}{\partial a}\sigma_a\right)^2+\left(\frac{\partial \mathrm{M}}{\partial b}\sigma_b\right)^2+0.5\left(\frac{\partial^2 \mathrm{M}}{\partial a^2}\sigma_a^2\right)^2+0.5\left(\frac{\partial^2 \mathrm{M}}{\partial b^2}\sigma_b^2\right)^2$$
$$+\left(\frac{\partial^2 \mathrm{M}}{\partial a\,\partial b}\sigma_a\sigma_b\right)^2. \tag{10}$$

Predictions of $\mathrm{M}(a,b)$, $\bar{\mathrm{M}}$ and σ_M for FOSM (Eqs. (7) and (9)) and SOSM (Eqs. (8) and (10)) are compared with CFD solutions and Monte Carlo analyses based on CFD solutions, as given and discussed in the results section.

3.2 Robust Shape Optimization. Applying the conventional optimization previously described yields
min Obj,

$$\text{Obj}=\text{Obj}(\mathrm{M},a,b)$$

subject to

$$\mathbf{R}(\mathbf{M},a,b)=0$$
$$V(a,b)\leq 0, \tag{11}$$

where the system constraint, V, is a constraint on the nozzle volume and depends only on a and b; our objective does not explicitly depend on $\mathbf{M}$.

Applying the robust optimization previously described yields
min Obj. $\quad \text{Obj}=\text{Obj}(\bar{\mathrm{M}},\sigma_M,\bar{a},\bar{b})$
subject to

$$\mathbf{R}(\bar{\mathbf{M}},\bar{a},\bar{b})=0$$
$$V(\bar{a},\bar{b})+k\sigma_V\leq 0, \tag{12}$$

where

$$\sigma_V^2=\left(\frac{\partial V}{\partial a}\sigma_a\right)^2+\left(\frac{\partial V}{\partial b}\sigma_b\right)^2. \tag{13}$$

With a and b subject to statistical uncertainties (which may be due to measurement, manufacturing, etc.), V becomes uncertain. Since V is linearly dependent on a and b, it is also normally distributed. Therefore, its standard deviation, σ_V, is given exactly by Eq. (13).

To demonstrate the optimizations, a simple target-matching problem is selected; a unique answer is obtained when an equality volume constraint is enforced. The CFD code is run for given a and b; the resulting $\mathbf{M}(a,b)$ and corresponding $V(a,b)$ are taken as the target values Mt and Vt, respectively. For this conventional optimization, the objective function and constraint function for V of Eq. (11) become

$$\text{Obj}(\mathrm{M},a,b)=[\mathrm{M}(a,b)-\mathrm{Mt}]^2$$
$$V(a,b)-\mathrm{Vt}=0$$

enforced as

$$V(a,b)-\mathrm{Vt}\leq 0 \text{ and } \mathrm{Vt}-V(a,b)\leq 0 \tag{14}$$

for the convenience of the optimizer.

For robust optimization using the FOSM approximation, the corresponding objective and constraint on V of Eq. (12) become

$$\text{Obj}(\bar{\mathrm{M}},\sigma_M,\bar{a},\bar{b})=[\bar{\mathrm{M}}(\bar{a},\bar{b})-\mathrm{Mt}]^2+\sigma_M^2$$
$$V(\bar{a},\bar{b})-\mathrm{Vt}+k\sigma_V=0$$

similarly enforced as

$$V(\bar{a},\bar{b})-\mathrm{Vt}+k\sigma_V\leq 0 \text{ and } \mathrm{Vt}-V(\bar{a},\bar{b})-k\sigma_V\leq 0. \tag{15}$$

Note that for $\sigma_a=\sigma_b=0$ in Eq. (15), the conventional optimization is obtained. Also, in the probabilistic statement of the constraint on V, it is assumed that the desired volume is less than or equal to Vt.

3.3 Flow Parameter Uncertainty Propagation. A second example of uncertainty in CFD involves fluctuations in input flow parameters. For the discussion of flow parameter uncertainty propagation, the free-stream Mach number, Minf, and the nozzle static back pressure, Pb, will be taken as statistically independent random variables. Specifying the free-stream Mach number sets the stagnation enthalpy. The Mach number distribution through the nozzle, M, is again viewed as a component of the state variable, Q; its value at the inlet, M, is the CFD output, F. Applying the approach previously outlined yields equations which are similar to Eq. (7) through (10) but with

Input random variables: $\mathbf{b}=\{\mathrm{Minf},\mathrm{Pb}\}$
CFD output function: $\mathbf{F}=\{\mathrm{M}\}$

Again, predictions of M, $\bar{\mathrm{M}}$, and σ_M for the FOSM and SOSM approximations are compared with CFD solutions and Monte Carlo analyses based on CFD solutions, as given and discussed in the next section.

3.4 Robust Design for Flow Control. The conventional optimization is expressed as

min Obj $\quad \text{Obj}=\text{Obj}(\mathrm{M},\mathrm{Minf},\mathrm{Pb})$
subject to

$$\mathbf{R}(\mathrm{M},\mathrm{Minf},\mathrm{Pb})=0$$
$$q(\mathrm{Minf},\mathrm{Pb})\leq 0, \tag{16}$$

where q is a constraint on the mass flux through the nozzle.

The robust optimization is expressed as

min Obj, $\quad \text{Obj}=\text{Obj}(\bar{\mathrm{M}},\sigma_M,\bar{\mathrm{M}}\mathrm{inf},\bar{\mathrm{P}}\mathrm{b})$
subject to

$$\mathbf{R}(\bar{\mathrm{M}},\bar{\mathrm{M}}\mathrm{inf},\bar{\mathrm{P}}\mathrm{b})=0$$
$$q(\bar{\mathrm{M}}\mathrm{inf},\bar{\mathrm{P}}\mathrm{b})+k\sigma_q\leq 0. \tag{17}$$

For the free-stream Mach number, Minf, and the nozzle back pressure, Pb, subject to statistical uncertainties, the mass flux, q, becomes uncertain. Since q is dependent on Minf and Pb, its standard deviation, σ_q, may be approximated by

$$\sigma_q^2=\left(\frac{\partial q}{\partial \mathrm{Minf}}\sigma_{\mathrm{Minf}}\right)^2+\left(\frac{\partial q}{\partial \mathrm{Pb}}\sigma_{\mathrm{Pb}}\right)^2. \tag{18}$$

Since q is not a linear function of Minf and Pb, Eq. (18) is not exact.

To demonstrate the optimizations, a simple target-matching problem is again chosen. The CFD code is run for given Minf and Pb, the resulting M and corresponding q are taken as the target values Mt and qt, respectively. For this conventional optimization, the objective function and constraint functions of Eq. (16) are

$$\text{Obj}(\mathrm{M}.\mathrm{Minf},\mathrm{Pb})=[\mathrm{M}(\mathrm{Minf},\mathrm{Pb})-\mathrm{Mt}]^2$$
$$q(\mathrm{Minf},\mathrm{Pb})-qt=0$$

enforced as

$$q(\mathrm{Minf},\mathrm{Pb})-qt\leq 0 \text{ and } qt-q(\mathrm{Minf},\mathrm{Pb})\leq 0. \tag{19}$$

For robust optimization using the FOSM approximation, the corresponding objective and constraint on q of Eq. (17) can be shown as

$$\text{Obj}=\text{Obj}(\bar{\mathrm{M}},\sigma_M,\bar{\mathrm{M}}\mathrm{inf},\bar{\mathrm{P}}\mathrm{b})=[\bar{\mathrm{M}}(\bar{\mathrm{M}}\mathrm{inf},\bar{\mathrm{P}}\mathrm{b})-\mathrm{Mt}]^2+\sigma_M^2$$
$$q(\bar{\mathrm{M}}\mathrm{inf},\bar{\mathrm{P}}\mathrm{b})-qt+k\sigma_q=0$$

enforced as

$$q(\bar{\mathrm{M}}\mathrm{inf},\bar{\mathrm{P}}\mathrm{b})-qt+k\sigma_q\leq 0 \text{ and } qt-q(\bar{\mathrm{M}}\mathrm{inf},\bar{\mathrm{P}}\mathrm{b})-k\sigma_q\leq 0. \tag{20}$$

Again note that for $\sigma_{\mathrm{Minf}}=\sigma_{\mathrm{Pb}}=0$ in Eq. (20), the conventional optimization is obtained. Also, in the probabilistic statement of the constraint on q, it is assumed that the desired mass flux is less than or equal to qt.

4 Sample Results and Discussion

Presentation and discussion of results for the sample quasi 1-D Euler CFD problems are divided into four topics: function approximations, uncertainty propagation, pdf approximations, and robust optimization. For the first three topics, the FOSM and SOSM approximations are assessed by comparison with direct CFD simulations. Note that the CFD code and its corresponding derivative codes are executed at the mean values of the random input variables to obtain the functions and sensitivity derivatives needed for construction of the statistical approximations.

4.1 Function Approximations. It is important to assess the Taylor series output function approximations with direct nonlinear CFD code simulations prior to presenting uncertainty propagation. If the CFD output function, M, is quasi-linear with respect to the input variables of interest, one can expect first-order approximations to be reasonably good; that is, the first-order moments given by Eq. (3) should match well with the moments produced by a Monte Carlo simulation. For a more nonlinear system, one naturally expects better accuracy with second-order approximations; that is, uncertainty analyses which include second-order terms should yield results which better predict the statistical moments produced by the Monte Carlo simulation.

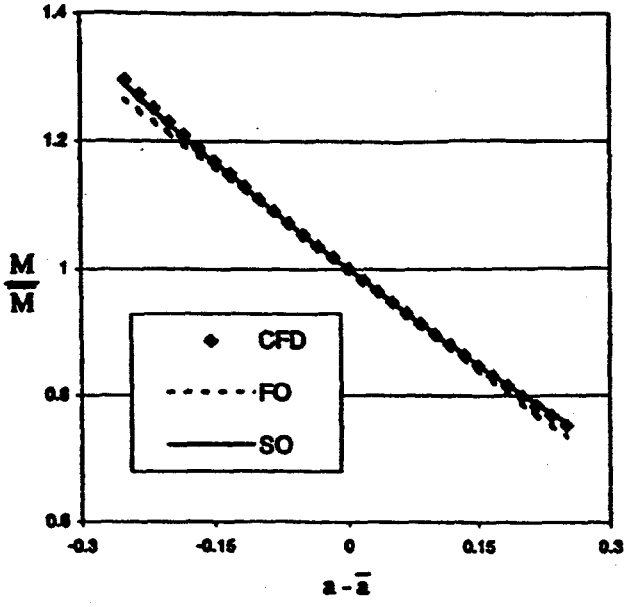

Fig. 1 Comparison of function approximations versus CFD solution, input variable $b=\bar{b}$

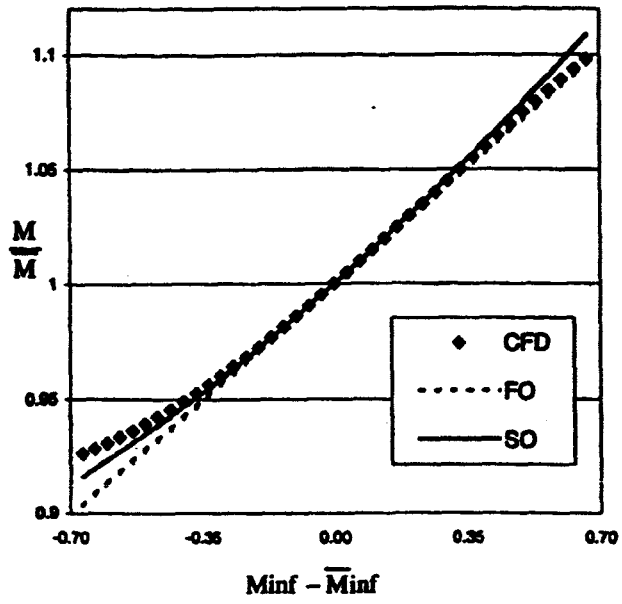

Fig. 3 Comparison of function approximations versus CFD solution, input variable Pb=P̄b

Figures 1–4 show that for $F=M(a,b)$, M behaves as a quasi-linear function in the neighborhood of $(\bar{a},\bar{b})$, whereas for $F=M(Minf,Pb)$, M is more nonlinear in the neighborhood of $(\bar{M}inf,\bar{P}b)$. In these figures, approximations of the CFD output functions, $M(a,b)$ and M(Minf,Pb), using the first- (FO) and second-order (SO) Taylor series (as given in Eqs. (7) and (8) for $M(a,b)$), are compared to direct solution of the Euler CFD. In each example, two traces were considered through the design space. Trace 1 varied the first input variable, while the second remained fixed at its mean value, and vice versa for trace 2. The required first- and second-order sensitivity derivatives needed for construction of the first-and second-order approximations were obtained by hand differentiation and automatic differentiation as discussed and presented in [12].

Nonlinear behavior of the CFD result is reasonably well approximated by the SO result in all plots; however, there does appear to be an inflection point in the CFD results given in Fig. 3. Note that the linear FO result is a good approximation in the geometric example; the flow parameter example is more nonlinear. At larger deviations from the mean, a linear approximation for M(Minf,Pb) loses accuracy.

4.2 Uncertainty Propagation. Approximation of the statistical first and second moments is done using equations Eq. (9) and (10) (geometric example), and corresponding equations for the flow parameter example. Again, both first- and second-order sensitivity derivatives are required and the prediction is straightforward, given these derivatives. An independent verification of these approximate mean and standard deviation values is obtained here using direct Monte Carlo (MC) simulation with the quasi 1-D Euler CFD code and standard statistical analyses of these Monte Carlo results. The standard statistical analyses used were from MicroSoft ® Excel 2000 and the random number generator MZRAN used was from [27]. Tables 1 and 2 give results for the mean (first moment) and Tables 3 and 4 give results for the stan-

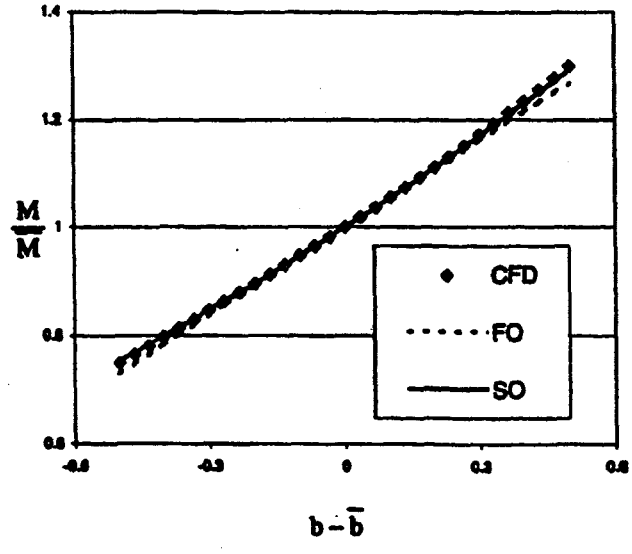

Fig. 2 Comparison of function approximations versus CFD solution, input variable $a=\bar{a}$

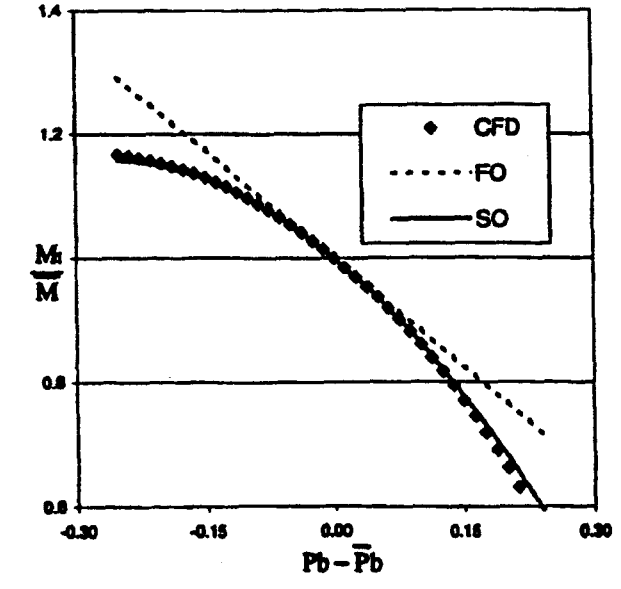

Fig. 4 Comparison of function approximations versus CFD solution, input variable Minf=Minf

Table 1 Percent difference from MC for FO and SO predictions of $\bar{M}$ ($\bar{a}$,$\bar{b}$)

Case	Input σ $\sigma_a=\sigma_b$	$\bar{M}$ MC	% Error MC	% diff w/MC FO Predict	% diff w/MC SO Predict
1	0.01	0.4041	0.0187	−0.0105	0.0656
2	0.02	0.4040	0.0379	0.0716	0.1531
3	0.04	0.4054	0.0756	−0.2867	0.0383
4	0.06	0.4055	0.1142	−0.3012	0.4301
5	0.08	0.4096	0.1557	−1.3078	−0.0209

Table 2 Percent difference from MC for FO and SO predictions of $\bar{M}$ ($\bar{M}$inf,$\bar{P}$b)

Case	Input σ $\sigma_{Minf}=\sigma_{Pb}$	$\bar{M}$ MC	% Error MC	% diff w/MC FO Predict	% diff w/MC SO Predict
1	0.01	0.3933	0.0056	0.0037	−0.0269
2	0.02	0.3932	0.0114	0.0187	−0.1034
3	0.04	0.3898	0.0229	0.8917	0.3991
4	0.06	0.3889	0.0364	1.1251	0.0141

Table 3 Percent difference from MC for FO and SO predictions of σ_M, geometric example

Case	Input σ $\sigma_a=\sigma_b$	σ_M MC	% diff w/MC FO Predict	% diff w/MC SO Predict
1	0.01	0.0102	−0.5773	−0.5708
2	0.02	0.0207	−1.7026	−1.6769
3	0.04	0.0414	−1.5794	−1.4766
4	0.06	0.0625	−2.2590	−2.0296
5	0.08	0.0853	−4.3987	−4.0001

Table 4 Percent difference from MC for FO and SO predictions of σ_M, flow parameter example

Case	Input σ $\sigma_{Minf}=\sigma_{Pb}$	σ_M MC	% diff w/MC FO Predict	% diff w/MC SO Predict
1	0.01	0.0030	1.1815	1.2473
2	0.02	0.0062	−1.5093	−1.2533
3	0.04	0.0125	−4.1604	−3.1680
4	0.06	0.0199	−4.4070	−2.1938

dard deviation (second moment) value comparisons. The input deviations (σ_a and σ_b) or (σ_{Minf} and σ_{Pb}), are taken to be equal and given in the second column of each table. The third column in each table gives the result from the MC simulation, where the sample size (N) used was 3000. The MC error in its predicted mean is $\sigma_M/\sqrt{N}$, which is given in the fourth column of Tables 1 and 2. The first-order (FO) and second-order (SO) approximate predictions are given in the last two columns of each table as percent difference from the MC results.

Results from the last two columns of Tables 1–4 are plotted in Figs. 5 and 6. Note that mean and standard deviation approximations for output M agree well with the MC results for small standard deviations in input variables, (σ_a,σ_b) or (σ_{Minf},σ_{Pb}), for both the FO and SO predictions. At higher standard deviations, the SO results tend to agree better with the MC results, especially in the flow parameter example.

As expected, the SO approximations are generally better than those for FO and an increase in the standard deviation of input parameters monotonically increases the error associated with both predictions. Both FO and SO approximations predict the mean more accurately than the standard derivation. Also note that the MC simulation with a sample size of 3000 limits accuracy of the MC results. This is apparent in the raggedness of the pdfs shown in the following section.

4.3 Probability Density Function Approximations. Given a mean and standard deviation of the CFD output function (from either an MC simulation or an FO or SO prediction) and assuming a normal distribution, one may then construct a pdf to approximate the behavior of the nondeterministic output function. This approximation is compared to pdf histograms generated from MC simulations in Figs. 7, 8, and 9. The bars depict the MC histogram, and the solid curve is a normal distribution at the MC mean value and MC standard deviation as given in the previous tables. The MC simulation size of 3000 is certainly not sufficient to obtain a smooth pdf. We note that both the first-order and second-order normal distributions are indistinguishable from this normal MC curve at this scale so neither is shown in the figure. It is apparent that for either the quasi-linear functional dependence on a and b (Fig. 7), or for small input standard deviations of the flow parameters (Fig. 8), the statistical approximations are good for a significant region about the mean but tend to break down in predicting the tails of the distribution. This is significant, for if one is primarily interested in reliable failure predictions, as for structural design, this prediction may not be good enough. It is felt, how-

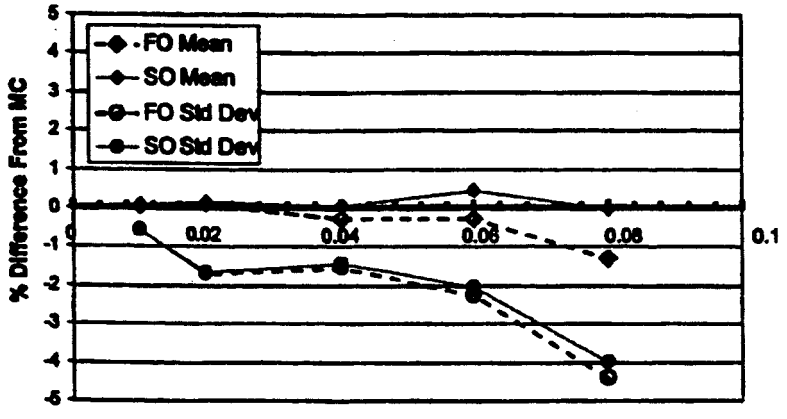

Fig. 5 Comparison of statistical moment approximations with Monte Carlo simulation results, geometric examples

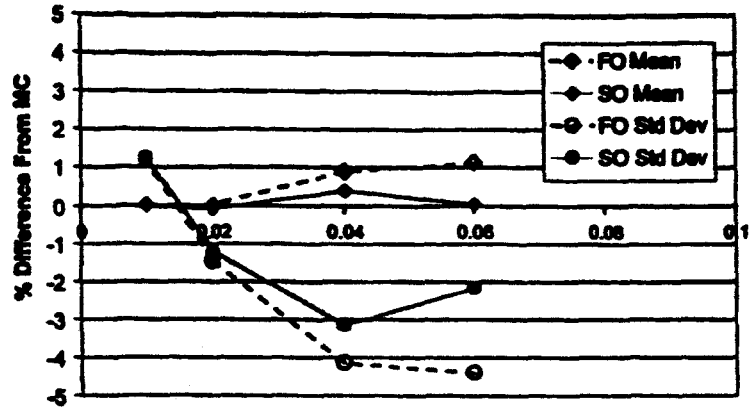

$$\sigma\left(\sigma_{\text{Minf}} = \sigma_{pb}\right)$$

Fig. 6 Comparison of statistical moment approximations with Monte Carlo simulation results, flow parameter examples

ever, that in aerodynamic performance optimization using CFD, where robustness about the mean is desired, these approximations may be good enough.

It is not surprising that a nonlinear CFD output function behaves differently for randomness in different input variables. For M(Minf,Pb) at higher input standard deviations ($\sigma_{\text{Minf}} = \sigma_{Pb} = 0.06$), the pdf of the output function is no longer normal. In Fig. 9 one can see the non-normal behavior of CFD output given normally distributed input variables Minf and Pb.

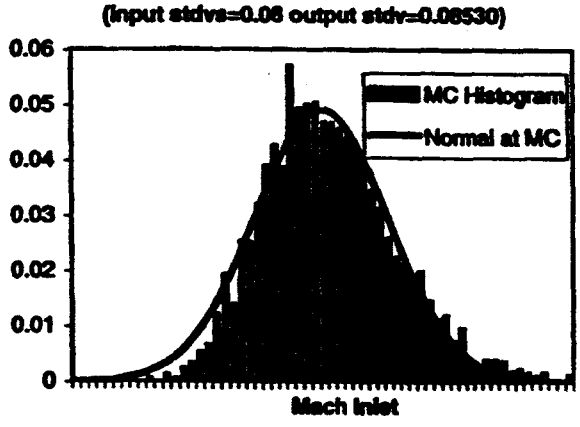

Fig. 7 Probability density function for M(a,b) for $\sigma_a = \sigma_b = 0.08$

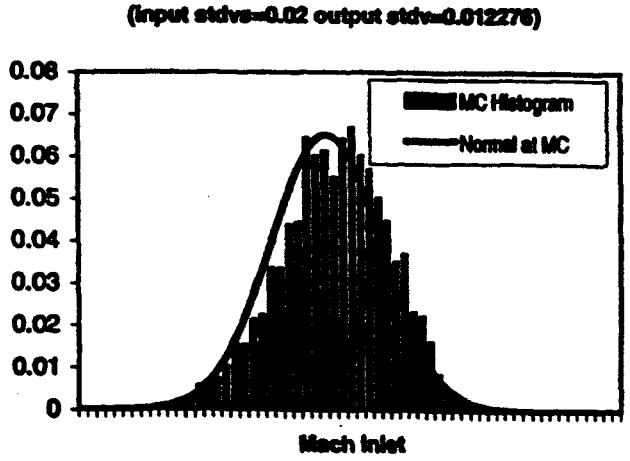

Fig. 8 Probability density function for M (Minf,Pb) for $\sigma_{\text{Minf}} = \sigma_{Pb} = 0.02$

4.4 Robust Optimizations. Optimization results were generated using the quasi 1-D Euler CFD code and the procedure given by Eqs. (5) and (6). As noted earlier, conventional optimization is obtained for $\sigma_a = \sigma_b = 0$ or for $\sigma_{\text{Minf}} = \sigma_{\text{Pb}} = 0$. For the FOSM approximation, first-order sensitivity derivatives are required to obtain σ_M and σ_V (Eqs. (9) and (13)) or σ_q (Eqs. (9) and (18)); therefore, second-order sensitivity derivatives will be required for their gradients, which are used in the optimization. The second-order derivatives were obtained by the manner presented in [12], except for those associated with Eq. (18) where the first-order derivatives were finite differenced simply for convenience.

It is seen from Eqs. (12) and (17) that the robust optimization results should depend on the probabilistic parameters (σ_a,σ_b) or (σ_{Minf},σ_{Pb}), and k. The desired probability, P_k, is that from the normal cumulative distribution function since σ_V and σ_q here are assumed to be normally distributed. For each robust optimization example, two cases are presented. For case 1, P_k is fixed at $k = 1$, i.e., $P_1 = 84.13\%$, and the effect of increasing the input variable standard deviations is addressed. For case 2, the standard deviations of the input variables are fixed at 0.01 and P_k increases.

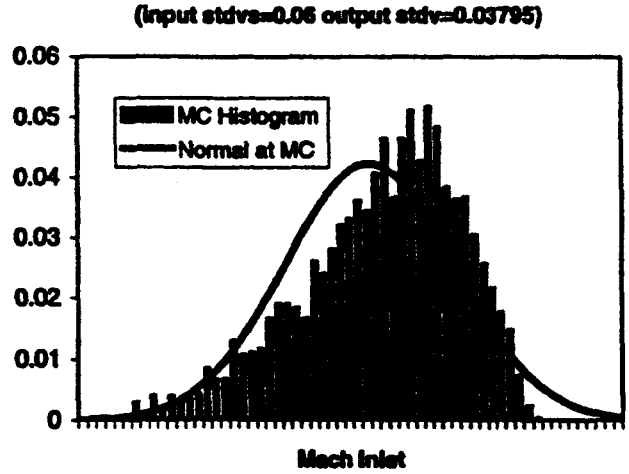

Fig. 9 Probability density function for M (Minf,Pb) for $\sigma_{\text{Minf}} = \sigma_{Pb} = 0.06$

Table 5 Robust shape optimization results with increasing input parameter σ for k=1

$\sigma_a=\sigma_b$	$\bar{a}$	$\bar{b}$	Obj	$\bar{M}$	σ_M	σ_V
0.00	0.6001	0.3001	0.0000	0.4043	0.0000	0.0000
0.02	0.6685	0.3667	0.0004	0.4036	0.0203	0.0120
0.04	0.7338	0.4286	0.0016	0.4018	0.0406	0.0240
0.06	0.7948	0.4841	0.0037	0.3984	0.0607	0.0360
0.08	0.8534	0.5358	0.0065	0.3941	0.0804	0.0480

Table 6 Robust shape optimization results with increasing P_k for σ=0.01

K	P_k	$\bar{a}$	$\bar{b}$	Obj	$\bar{M}$	σ_M	σ_V
0	0.5000	0.5996	0.2995	0.000104	0.4041	0.0101	0.006
1	0.8413	0.6246	0.3189	0.000118	0.4004	0.0101	0.006
2	0.9772	0.6698	0.3687	0.000104	0.4041	0.0101	0.006
3	0.9986	0.7052	0.4037	0.000104	0.4042	0.0102	0.006
4	0.9999	0.7406	0.4388	0.000104	0.4043	0.0102	0.006

4.4.1 Robust Shape Optimization Results. In Table 5, results for case 1 of the robust shape optimization are displayed. For $\sigma_a=\sigma_b$ ranging from 0 to 0.08, optimal values for the input variables $(\bar{a},\bar{b})$ are listed. As $\sigma_a=\sigma_b$ increases, so does σ_V. Accordingly, the mean values, $(\bar{a},\bar{b})$, which minimize the objective function and satisfy the probabilistic constraint, become increasingly displaced from the target volume, Vt. This is shown in Fig. 10. Mean values $(\bar{a},\bar{b})$ change, keeping the mean value, $\bar{M}(\bar{a},\bar{b})$, of the probabilistic output near the target value, Mt. The robust design points track the dashed curve for $\bar{M}$=Mt with some displacement due to the $\sigma_M{}^2$ term of the objective, Eq. (15). The volume, $V(\bar{a},\bar{b})$, is displaced from the solid curve V=Vt by $k\sigma_V$, as required by the probabilistic constraint. This displacement can be viewed as the solution dependent or "effective" safety factor.

In Fig. 11 the changing area distribution of the robust optimization is illustrated. As the standard deviations of design variables $(\bar{a},\bar{b})$ increase, the optimal nondeterministic volume, $V(\bar{a},\bar{b})$, significantly decreases.

The results for case 2 of the robust shape optimization, where $\sigma_a=\sigma_b$ is fixed at 0.01, and P_k increases from 50 percent to 99.99 percent (k=0 to 4) are given in Table 6. Again mean values $(\bar{a},\bar{b})$ change, keeping the mean value, $\bar{M}(\bar{a},\bar{b})$, of the probabilistic output near the target value, Mt. Since $\sigma_a=\sigma_b$ remains small, the σ_M^2 term of the objective remains small, and the displacement of $\bar{M}$ from the dashed line depicting Mt due to the σ_M^2 term remains small as shown in Fig. 12. With an increase in P_k, $V(\bar{a},\bar{b})$ is displaced from the solid curve V=Vt by $k\sigma_V$, as required by the probabilistic constraint. Accordingly, the mean values, $(\bar{a},\bar{b})$, which minimize the objective function and satisfy the constraint, again become increasingly displaced from those at the target volume, Vt. Note the significant displacement of the solution from the target volume when P_k is large, i.e., when one is attempting to incorporate the tails of the pdf. In order to increase the probability of constraint satisfaction from 97.77 percent to 99.99 percent, one sees a significant change in $(\bar{a},\bar{b})$ for a mere gain of 2 percent in constraint satisfaction.

4.4.2 Robust Design for Flow Control Results. Similar results are seen in the flow parameter example. In Table 7, the

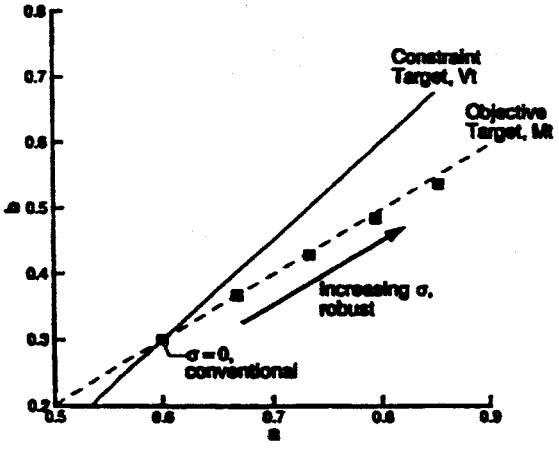

Fig. 10 Optimization results in design space (a,b), P_k fixed at P_1

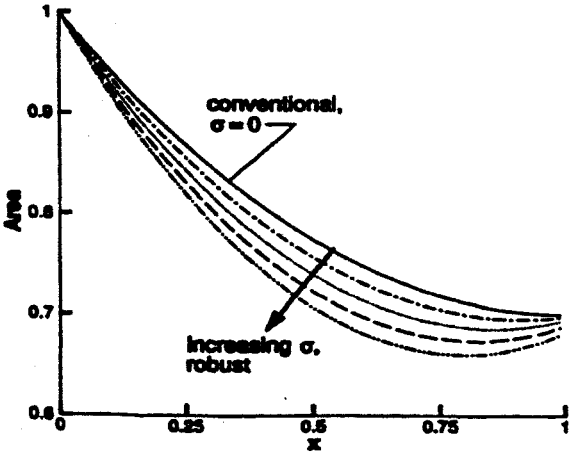

Fig. 11 Nozzle area distributions, P_k fixed at P_1

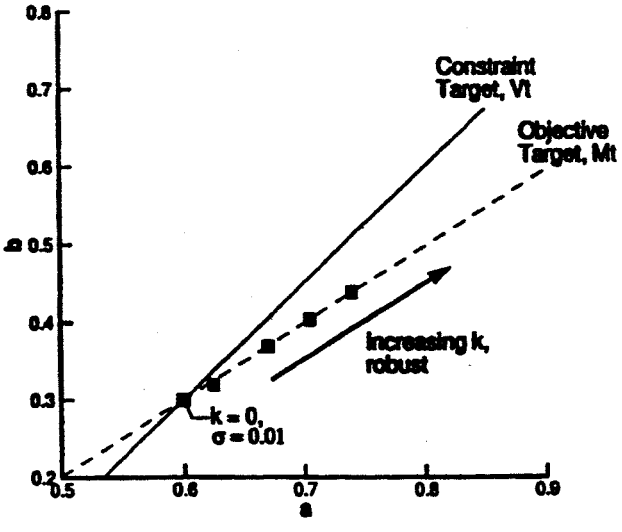

Fig. 12 Optimization results in design space (a,b), σ fixed at 0.01

Table 7 Robust design for flow control results with increasing input parameter σ for k=1

$\sigma_{Min}=\sigma_{Pb}$	Minf	Pb	Obj	$\bar{M}$	σ_M	σ_q
0	0.3000	0.8000	0.0000	0.3933	0.0000	0.0000
0.02	0.2861	0.7883	0.0001	0.3974	0.0116	0.0058
0.04	0.2655	0.7801	0.0005	0.3985	0.0231	0.0112
0.06	0.2555	0.7653	0.0012	0.4050	0.0327	0.0163
0.08	0.2468	0.7498	0.0020	0.4118	0.0407	0.0209

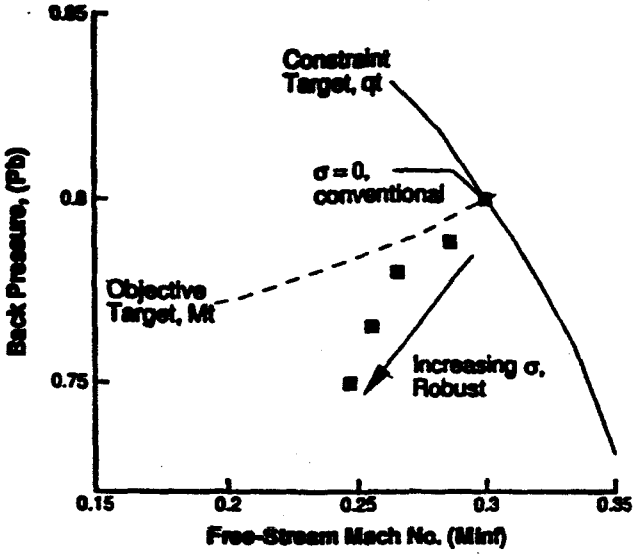

Fig. 13 Optimization results in design space (Minf,Pb), P_k fixed at P_1

results for case 1 are displayed. For $\sigma_{Minf}=\sigma_{Pb}$ ranging from 0 to 0.08, optimal values for the input variables ($\bar{M}$inf,$\bar{P}$b) are listed. As $\sigma_{Minf}=\sigma_{Pb}$ increases, so does σ_q. Accordingly, the mean values, ($\bar{M}$inf,$\bar{P}$b), which minimize the objective function and satisfy the constraint, become increasingly displaced from the target mass flux, qt. This is shown in Fig. 13. Mean values ($\bar{M}$inf,$\bar{P}$b) change, keeping the mean value, $\bar{M}$($\bar{M}$inf,$\bar{P}$b), of the probabilistic output near the target value, Mt. The robust design points track the dashed curve for $\bar{M}$=Mt with displacement due to the σ_M^2 term of the objective, Eq. (17). The optimized mass flux, $q(\bar{M}inf,\bar{P}b)$, is displaced from the solid curve $q=qt$ by $k\sigma_q$ as required by the probabilistic constraint.

Table 8 Robust design for flow control results with increasing P_k for σ=0.01

K	P_k	$\bar{M}$inf	$\bar{P}$b	Obj	$\bar{M}$	σ_M	σ_q
0	0.5000	0.3000	0.8000	0.00003	0.3933	0.0060	0.0030
1	0.8413	0.2919	0.7953	0.00003	0.3945	0.0059	0.0029
2	0.9772	0.2825	0.7916	0.00003	0.3949	0.0059	0.0029
3	0.9986	0.2688	0.7896	0.00003	0.3936	0.0060	0.0028
4	0.9999	0.2598	0.7867	0.00003	0.3938	0.0060	0.0028

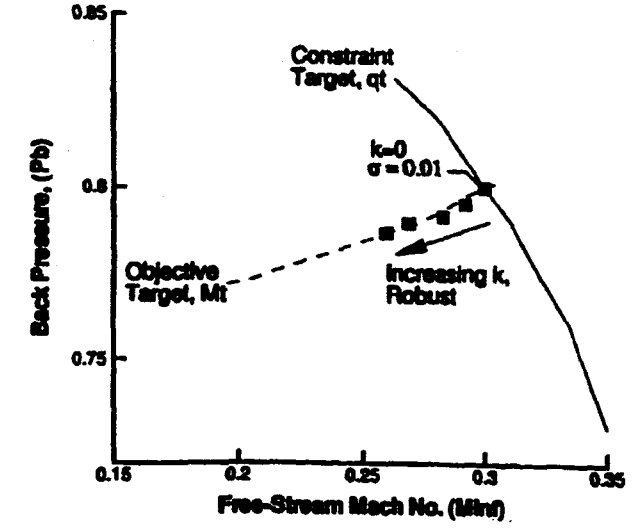

Fig. 14 Optimization results in design space (Minf,Pb), σ fixed at 0.01

The results for case 2 of the robust design for flow control, where $\sigma_{Minf}=\sigma_{Pb}$ is fixed at 0.01, and P_k increases from 50 percent to 99.99 percent, (k=0 to 4) are given in Table 8. Again, mean values ($\bar{M}$inf,$\bar{P}$b) change, keeping the mean value, $\bar{M}$($\bar{M}$inf,$\bar{P}$b), of the probabilistic output near the target value, Mt. As in the preceding example, since $\sigma_{Minf}=\sigma_{Pb}$ remains small, the σ_M^2 term of the objective remains small and the displacement due to the σ_M^2 term remains small, as shown in Fig. 14. With an increase in P_k, $q(\bar{M}inf,\bar{P}b)$ is displaced from the solid curve $q=qt$ by $k\sigma_q$, as required by the probabilistic constraint. Accordingly, the mean values, ($\bar{M}$inf,$\bar{P}$b), which minimize the objective function and satisfy the constraint again become increasingly displaced from the target mass flux, qt. Again, note the significant displacement from the target mass flux incurred in the higher probability optimizations, i.e., when one is attempting to incorporate the tails of the pdf.

5 Concluding Remarks and Challenges

The present results represent an implementation of the approximate statistical moment method for uncertainty propagation and robust optimization for a quasi 1-D Euler CFD code. Assuming statistically independent, random, normally distributed input variables, first- and second-order statistical moment procedures were performed to approximate the uncertainty in the CFD output. Efficient calculation of both first- and second-order sensitivity derivatives was employed and the validity of the approximations was assessed by comparison with statistical moments generated through Monte Carlo simulations. The uncertainties in the CFD input variables were incorporated into a robust optimization procedure where statistical moments involving first-order sensitivity derivatives appeared in the objective function and system constraints. Second-order sensitivity derivatives were used in a gradient-based robust optimization. The approximate methods used throughout the analyses were found to be valid when considering robustness about input parameter mean values.

Collectively, these results demonstrate the possibility for an approach to treat input parameter uncertainty and its propagation in gradient-based design optimization that is governed by complex CFD analysis solutions. It has been demonstrated on a very simple CFD code and problem; there are computational resource issues to be addressed in application to significant 2-D and 3-D CFD codes and problems. Conventional optimization in 2-D and 3-D already requires significantly more resources than in 1-D and obtaining second-order sensitivity derivatives for more design variables will add even more work. Some of these are addressed in [12] and work is presently in progress regarding application and demonstration using 2-D and 3-D Euler CFD code.

Acknowledgments

The authors wish to thank Dr. Luc Huyse of the Institute for Computer Applications in Science and Engineering (ICASE) at NASA Langley for many helpful discussions regarding statistical aspects related to this study, and also Dr. Thomas Zang of the Multidisciplinary Optimization Branch at NASA Langley for his encouragement and support. One author (ACT III) was partially supported by an ASEE Grant during the summer of 2000 at NASA Langley.

Nomenclature

A = nozzle area
a = geometric shape parameter
b = geometric shape parameter
$\mathbf{b}$ = vector of independent input variables

$\mathbf{F}$ = vector of CFD output functions
g = vector of conventional optimization constraints
k = number of standard deviations
M = Mach number at nozzle inlet
$\mathbf{M}$ = vector of Mach number at each grid point
Minf = free-stream Mach number
Mt = target inlet Mach number
N = Monte Carlo sample size
Pb = normalized nozzle static back (outlet) pressure
$\mathbf{Q}$ = vector of flow-field variables (state variables)
q = mass flux through nozzle
qt = target mass flux through nozzle
$\mathbf{R}$ = vector of state equation residuals
V = nozzle volume
Vt = target nozzle volume used for optimization
x = normalized axial position within nozzle
σ = standard deviation
σ^2 = variance

Superscript

- = mean value

Appendix-Quasi One-Dimensional Euler CFD

The steady-state, quasi 1-D Euler equations are

$$\frac{\partial E(Q)}{\partial x}+S(Q)=0$$

where

$$Q=[\rho,\rho u,\rho e_0]^T,$$

$$E(Q)=[\rho u,\rho u^2+P,(\rho e_0+P)u]^T,$$

$$S(Q)=-\frac{dA}{dx}\frac{1}{A}[\rho u,\rho u^2,(\rho e_0+P)u]^T.$$

In these equations, ρ is density, u is flow speed, P is pressure, e_0 is the specific total energy (i.e., $e_0=e+u^2/2$, where e is the specific internal energy), and $A(x)$ is the local cross-sectional area. The ideal gas law with a constant ratio of specific heats γ (taken to be 1.4) is used for closure, which implies $P=(\gamma-1)(\rho e_0-\rho u^2/2)$. The governing equations are discretized and solved numerically with the upwind flux-vector-splitting method of Van Leer [28], which includes the use of higher order accuracy to approximate the flux terms. A more complete discussion of these numerical procedures is presented in [29]. The flow field was discretized with 100 grid points. This discretiztion of the governing equations, together with the numerical treatment of the boundary conditions, results in a large set of coupled nonlinear algebraic equations with the form of Eq. (5). In this study, the procedure for solving the discrete nonlinear flow equations is Newton's method.

References

[1] Newman, P. A., Hou, G. J.-W., and Taylor, A. C., III, 1997 "Observations Regarding Use of Advanced CFD Analysis, Sensitivity Analysis, and Design Codes in MDO." N.M. Alexandrov, and M.Y. Hussaini, eds., *Multidisciplinary Design Optimization: State of the Art*, SIAM Proceedings Series, SIAM, Philadelphia, pp. 263–279; also ICASE Report 96-16, NASA CR 198293 (available electronically at www.icase.edu).

[2] Newman, J. C., III, Taylor, A. C., III, Barnwell, R. W., Newman, P. A., and Hou, G. J.-W., 1999, "Overview of Sensitivity Analysis and Shape Optimization for Complex Aerodynamic Configurations," J. Aircr., **36**, No. 1, pp. 87–96.

[3] Jameson, A., and Vassberg, J. C., 2001, "Computational Fluid Dynamics for Aerodynamic Design: Its Current and Future Impact," AIAA-2001-0538, Jan.

[4] Thanedar, P. B., and Kodiyalam, S., 1992, "Structural Optimization Using Probabilistic Constraints," Struct. Optim., **4**, pp. 236–240 (also AIAA-91-0922-CP, 1991).

[5] Parkinson, A., Sorensen, C., and Pourhassan, N., 1993, "A General Approach for Robust Optimal Design," ASME J. Mech. Des., **115**, No. 1, pp. 74–80.

[6] Chen, X., Hasselman, T. K., and Neill, D. J., 1997, "Reliability Based Structural Design Optimization for Practical Applications," AIAA-97-1403, Apr.

[7] Du, X., and Chen, W., 1999, "Towards a Better Understanding of Modeling Feasibility Robustness in Engineering Design," American Society of Mechanical Engineers, Paper DAC-8565, Sept.

[8] A Collection of Technical Papers, 40th AIAA/ASME/ASCE/AHS/ASC Structures, Structural Dynamics, and Materials Conference and Exhibit, AIAA Forum on Non-Deterministic Approaches, St. Louis, MO, April 12–15, 1999.

[9] Chinchalkar, S., and Taylor, D. L., 1994, "Geometric Uncertainties in Finite Element Analysis," Computing Systems in Engineering, **5**, No. 2, pp. 159–170.

[10] Du, X., and Chen, W., 2000, "Methodology for Managing the Effect of Uncertainty in Simulation-Based Design," AIAA J., **38**, No. 8, pp. 1471–1478.

[11] Turgeon, E., Pelletier, D., and Borggaard, J., 2001, "Sensitivity and Uncertainty Analysis for Variable Property Flows," AIAA 2001-0139, Jan.

[12] Taylor, A. C., III, Green, L. L., Newman, P. A., and Putko, M. M., "Some Advanced Concepts in Discrete Aerodynamic Sensitivity Analysis," AIAA-2001-2529.

[13] Sherman, L., Taylor, A., III, Green, L., Newman, P., Hou, G., and Korivi, M., 1996, "First-and Second-Order Aerodynamic Sensitivity Derivatives via Automatic Differentiation with Incremental Iterative Methods," J. Comput. Phys., **129**, No. 2, pp. 307–336.

[14] Huyse, L., and Lewis, R. M., 2001, "Aerodynamic Shape Optimization of Two-dimensional Airfoils Under Uncertain Conditions," ICASE Report No. 2001-1, NASA CR-2001-210648, Jan.

[15] Huyse, L., 2001, "Solving Problems of Optimization Under Uncertainty as Statistical Decision Problems," AIAA 2001-1519, Apr.

[16] Oakley, D. R., Sues, R. H., and Rhodes, G. S., 1998, "Performance Optimization of Multidisciplinary Mechanical Systems Subject to Uncertainties," Probabilistic Engineering Mechanics, **13**, No. 1, pp. 15–26.

[17] Alvin, K. F., Oberkampf, W. L., Rutherford, B. M., and Diegert, K. V., 2000, "Methodology for Chacterizing Modeling and Discretization Uncertainties in Computational Simulation," Sandia Report SAND2000-5015, Mar.

[18] Oberkampf, W. L., DeLand, S. M., Rutherford, B. M., Diegert, K. V., and Alvin, K. F., 1999, "A New Methodology for the Estimation of Total Uncertainty in Computational Simulation," AIAA-99-1612, Apr. (see Ref. [8], pp. 3061–3083).

[19] Green, L. L., Newman, P. A., and Haigler, K. J., 1996, "Sensitivity Derivatives for Advanced CFD Algorithm and Viscous Modeling Parameters via Automatic Differentiation," J. Comput. Phys., **125**, No. 2, pp. 313–324 (also AIAA 93-3321).

[20] Robinson, D. G., 1998, "A Survey of Probabilistic Methods Used in Reliability, Risk and Uncertainty Analysis: Analytical Techniques I," Sandia Report SAND98-1189, June.

[21] Bischof, C. H., Carle, A., Corliss, G. F., Griewank, A., and Hovland, P., 1992, "ADIFOR: Generating Derivative Codes from Fortran Programs," Sci. Prog., **1**, No. 1, pp. 1–29.

[22] Bischof, C., Carle, A., Khademi, P., and Mauer, A., 1996, "Automatic Differentiation of FORTRAN," IEEE Comput. Sci. Eng., Fall.

[23] Carle, A., and Fagan, M., 2000, "Overview of Adifor 3.0," Department of Computational and Applied Mathematics, Rice University, CAAM-TR 00-02, Jan.

[24] Anon., 1995, *Design Optimization Tools-DOT Users Manual: Version 4.20*, Vanderplaats Research & Development, Inc., Colorado Springs, May.

[25] Dadone, A., Valorani, M., and Grossman, B., 2000, "Smoothed Sensitivity Equation Method for Fluid Dynamic Design Problems," AIAA J., **38**, No. 3, pp. 418–426.

[26] Zhang, X., Pelletier, D., Trepanier, J., and Camarero, R., 2000, "Verification of Error Estimators for the Euler Equations," AIAA-2000-1001, Jan.

[27] Marsaglia, G., and Zaman, A., 1994, "Some Portable Very-Long-Period Random Number Generators," Comput. Phys., **8**, No. 1, pp. 117–121.

[28] Van Leer, B., 1982, "Flux-Vector Splitting for Euler Equations," ICASE Report 82-30, Sept. (Also *Lecture Notes in Physics*, **170**, pp. 507–512, 1982).

[29] Thomas, J. L., Van Leer, B., and Walters, R. W., 1990, "Implicit Flux-Split Schemes for the Euler Equations," AIAA J., **28**, pp. 973–974.